Enhanced Light-Harvesting by Integrating Synergetic Microcavity and Plasmonic Effects for High-Performance ITO-Free Flexible Polymer Solar Cells

*Kai Yao, Xu-Kai Xin, Chu-Chen Chueh, Kung-Shih Chen, Yun-Xiang Xu, and Alex K.-Y. Jen**

In this work, a high-performance ITO-free flexible polymer solar cell (PSC) is successfully described by integrating the plasmonic effect into the ITO-free microcavity architecture. By carefully controlling the sizes of embedded Ag nanoprisms and their doping positons in the stratified device, a significant enhancement in power conversion efficiency (PCE) is shown from 8.5% (reference microcavity architecture) to 9.4% on flexible substrates. The well-manipulated plasmonic resonances introduced by the embedded Ag nanoprisms with different LSPR peaks allow the complementary light-harvesting with microcavity resonance in the regions of 400–500 nm and 600–700 nm, resulting in the substantially increased photocurrent. This result not only signifies that the spectral matching between the LSPR peaks of Ag nanoprisms and the relatively low absorption response of photoactive layer in the microcavity architecture is an effective strategy to enhance light-harvesting across its absorption region, but also demonstrates the promise of tailoring two different resonance bands in a synergistic manner at desired wavelength region to enhance the efficiency of PSCs.

1. Introduction

Optical engineering has been proven as a very powerful tool to improve the light-harvesting efficiency and power conversion efficiencies (PCEs) of organic photovoltaics (OPVs).[1–8] With respect to the nature of low carrier mobility and short exciton diffusion length of organic absorbers,[9] the optimum thickness of a photoactive layer is usually restricted to ≈100 nm in order to mitigate the charge recombination loss, which rises significantly as film thickness increases.[10] Consequently, this thin-film structure will encounter a huge optical transmission dissipation and hamper the photocurrent generation.[1] In this regard, numerous optical engineering strategies including the use of tandem structures,[3] resonant cavities,[6,7] photonic crystals,[4] metal nanogratings,[5] and metal nanoparticles[8] have been considerably exploited to enhance the light absorption of OPVs and enable high external quantum efficiencies (EQE) out from such thin-film structures.

All these approaches enhance the optical density in photoactive layer through different mechanisms. The tandem structures consisting of mutli-junction stacking are well known to extend the light-harvesting of devices by the complementary absorption from constituent BHJs with distinct band gaps.[3] For resonant cavity, it increases the optical density by prolonging the pathways of incident lights (with certain resonant frequencies) through optical confinement since the optical resonance occurs while optical waves formed from multiple reflections at metal layers constructively interfere.[6,7,11–13] Such optical microcavity has been successfully employed as an efficient light-trapping technique in ITO-free OPVs, especially for the thin photoactive layer due to its intense resonant coherence.[6,7,11–13]

We have recently revealed that the ITO-free device adopting microcavity configuration (shown in **Figure 1**B),[13b] where the optical microcavity is formed between top thin Ag and bottom opaque Ag electrodes due to highly reflective properties of Ag,[14] can demonstrate an improved PCE up to 8.6% compared to the ITO-based counterpart (7.7%, as shown in Figure 1A).[13] It is worth to note that the thin Ag electrode possessing high transmittance and low sheet resistance can replace ITO to enable the fabrication of high-performance flexible OPVs with good bending durability.[13,15] However, the enhanced light-matter interactions induced by such optical microcavity is strongly dependent on the resonant frequencies/wavelengths.[16] Owning to this wavelength dependence of constructive interference, the optical loss of the out-of-phase wavelengths will unavoidably increase either by reflection or transmission.[13] A representative EQE of microcavity device inserted in Figure 1 clearly manifests this phenomenon, in which the EQE enhancement is only observed for the resonance region ranging from 500 nm to 650 nm while the rest of wavelengths show suppressed response.[13]

Dr. K. Yao, Dr. X.-K. Xin, Dr. C.-C. Chueh, Dr. K.-S. Chen, Dr. Y.-X. Xu, Prof. A. K.-Y. Jen
Department of Materials Science and Engineering
University of Washington
Seattle, WA 98195, United States
E-mail: ajen@u.washington.edu

Dr. K. Yao
Institute of Photovoltaics/Department of Materials Science and Engineering
Nanchang University
999 Xuefu Avenue, Nanchang 330031, China

DOI: 10.1002/adfm.201403297

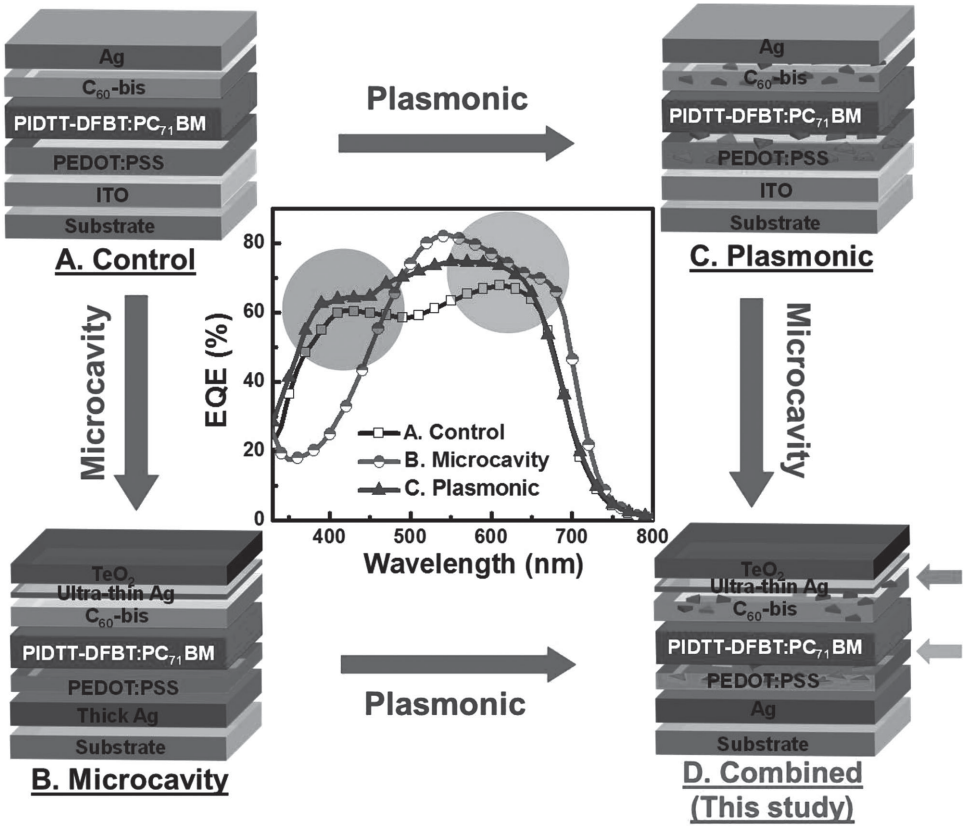

Figure 1. A) Normal ITO-based configuration (bottom illumination). B) Top-illuminated microcavity device.[13b] C) Plasmonic device incorporating Ag nanoprisms into charge transport interlayers (bottom illumination).[21b] D) Top-illuminated microcavity device adopting plasmonic effects, a combined device structure of (B) and (C). The central EQE spectra manifests the proposed strategy to compensate the light-harvesting of microcavity device by introducing plasmonic effects via doping spectral tuning nanoprisms into front (blue) and rear (green) charge transport interlayers.

In addition to tandem structures and optical microcavity, localized surface plasmon resonance (LSPR) (usually introduced by metal nanoparticles (NPs)) is another attractive approach to enhance the light-trapping of OPVs.[8,17] In principle, the resonant wavelengths of plasmonic effects can be manipulated by controlling the NPs' sizes, geometries, and the local dielectric environment.[18,19] Therefore, it is practical to spectrally match the absorption of photoactive layers to enrich the light-harvesting efficiency of OPVs.[20] Lately, we have also shown that the enhanced light absorption with tailorable wavelengths can be achieved by fine-tuning the size/shape of metal NPs embedded in the charge-transporting interlayers as a result of their associated plasmon resonance bands (Figure 1C).[21] Standing on this principle, we are particularly interested in further extending the light absorption of microcavity devices by introducing the LSPR effects to compensate the wavelength regions with relatively poor light absorption in the microcavity structures, as proposed in Figure 1D.

In this paper, we have successfully demonstrated a high-performance ITO-free flexible polymer solar cell by integrating the microcavity and plasmonic effects. Due to the synergetic resonant coherence, a broadband and high absorption response of photoactive layer can be accomplished. Given this appreciable enhancement in light-harvesting, an ITO-free flexible device with a PCE_{MAX} of up to 9.4% is demonstrated, which is substantially improved compared to the reference device only adopting microcavity configuration (PCE_{MAX}: 8.5%) and the normal ITO-based counterpart (PCE_{MAX}: 7.2%). This result not only demonstrates the state-of-the-art PCE for flexible OPVs but also manifests the feasibility of combing two different resonance bands in a compatible method for enhancing the light absorption of active layers.

2. Results and Discussion

Extended from our previous works, high-efficiency BHJ consisting of ladder-type donor polymer, poly(indaceno-dithieno[3,2-b]thiophene difluorobenzothiadiazole) (PIDTT-DFBT), and [6,6]-phenyl-C_{71}-butyric acid methyl ester ($PC_{71}BM$) as well as C_{60}-bis surfactant were chosen for further investigation as photoactive layer and electron transporting layer, respectively.[13b,21b,22] The detailed chemical structures of these materials were shown in Scheme S1. The silver nanoprisms used in this work were synthesized following a thermally induced synthesis method[23] and denoted as Ag-λ, where λ indicates the corresponding LSPR peak position in solution. As displayed in **Figure 2**A–B, the larger prisms feature red-shifted extinction spectra,[24] which affirms that the optical properties of Ag nanoprisms can be tailored by controlling their size/shape. To spectrally

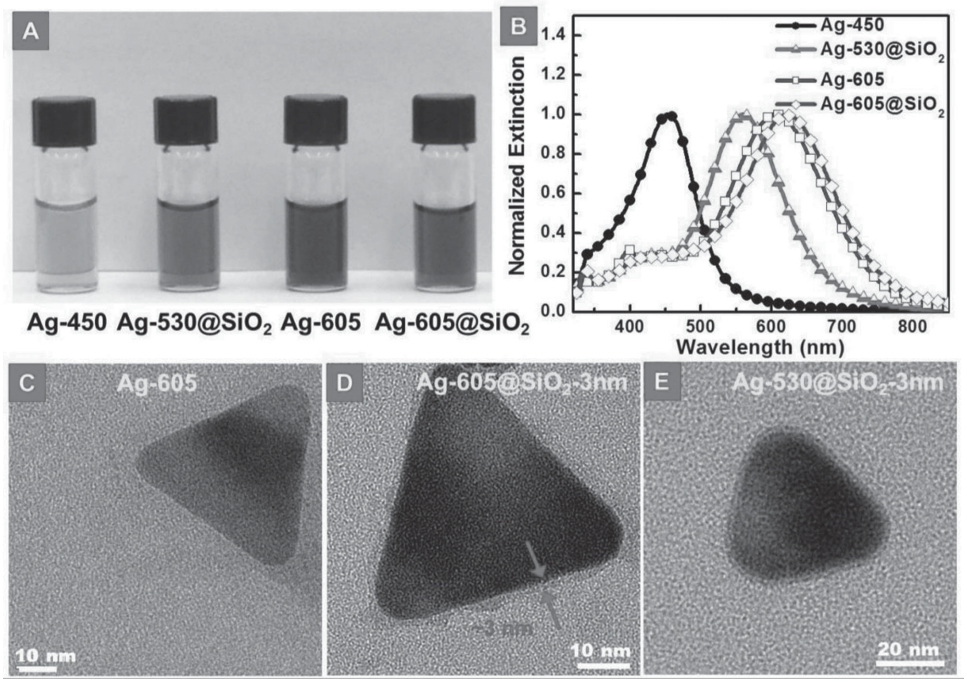

Figure 2. A) Size series, B) normalized extinction, and C–E) HR-TEM images of studied colloidal Ag nanoprisms with different extinction peaks. For the extinction spectra, Ag-605, Ag-605@SiO_2, and Ag-530@SiO_2 dissolve in water while Ag-450 dissolves in methanol.

match the LSPR peaks with the relatively low absorption response of BHJ layer in the microcavity device (EQE shown in Figure 1), two nanoprisms, Ag-450 and Ag-605 with edge length around 20 nm and 55 nm were chosen for plasmonic enhancement while Ag-530 was also prepared for comparison. Note that these Ag nanoprisms were further encapsulated with a thin silica shell (≈3 nm) via a sol–gel process as shown in Figure 2C-E in order to avoid the charge recombination and exciton quenching at metal surface (the detailed information is described in Figure S1, Supporting Information). In addition to the size effects, the LSPR peaks of Ag nanoprisms are also strongly correlated with the surrounding dielectric environments. Owing to the dielectric constant change caused by the silica shell, Ag-605@SiO_2 exhibits a red-shifted LSPR peak to 625 nm compared to pristine Ag-605 (Figure 2B).[25] Moreover, the LSPR peak of Ag-605@SiO_2 is further red-shifted to 650 nm in PEDOT:PSS due to higher refractive index ($n_{average}$ ≈ 1.4) of PEDOT:PSS (Figure S2 and Table S1, Supporting Information). The AFM images shown in Figure S3, Supporting Information, verify that Ag nanoprisms were not clustered in PEDOT:PSS and caused negligible change on BHJ morphology/thickness.[26]

The configuration of reference device employing microcavity structure in this work is: substrates/Ag (120 nm)/PEDOT:PSS (25 nm)/PIDTT-DFBT:$PC_{71}BM$ (90 nm)/C_{60}-bis (15 nm)/Ag (15 nm)/TeO_2 (50 nm).[13b] Note that an additional top-capping TeO_2 layer is essentially required on top of semi-transparent Ag electrode to heighten the electric field distribution within device because it can serve as an optical spacer and light in-coupling layer to relieve the optical dissipation induced by Ag reflection.[27] The optimized reference device showed an average PCE of 8.36 ± 0.16% with a short-circuit current density (J_{sc}) of 14.47 mA cm^{-2}, an open-circuit voltage (V_{oc}) of 0.96 V, and a fill factor (FF) of 0.60 (**Table 1**). More details regarding on optimization of such top-illuminated ITO-free structure can be found in our recent work.[13] It is important to notice that the optimized thickness of PEDOT:PSS layer is 25 nm, only half of the value for normal ITO-based device. As illustrated in Figure S4, Supporting Information, the electric field distribution across BHJ layer is strongly dependent on the thickness of PEDOT:PSS layer.[11] The microcavity enhancement becomes evanescent while the thickness of PEDOT:PSS layer increases from 25 nm to 50 nm, and thus results in a decreased photocurrent and PCE (Figure S5, Supporting Information).

To couple the plasmonic effects with optical microcavity, we fabricated three types of "combined" devices by integrating Ag nanoprisms into different interfacial layers: 1) in PEDOT:PSS at the rear side of device (denoted as rear-side type), 2) in C_{60}-bis at the front side of device (denoted as front-side type), and 3) in both interfacial layers (denoted as dual type). In principle, it is desirable to introduce the plasmonic enhancement with different LSPR resonance into the microcavity structure simultaneously to increase the absorption region around 450 nm as well as 650 nm (Figure 1). Limited by the thin thickness of C_{60}-bis (15 nm), it would be more rational to blend large Ag-605 into PEDOT:PSS layer while blending small Ag-450 into C_{60}-bis layer.[21b] Nevertheless, given that the edge length of Ag-605 (55 nm) was twice as large as the optimized thickness of PEDOT:PSS layer (25 nm), a thin silica shell around the Ag nanoprisms was essential to avoid the direct contact with BHJ layer. The bare nanoprisms in direct contact with BHJ layer will induce significant charge recombination or exciton quenching losses at metal surfaces.[28] It is also evident in the poor performance of the rear-side device with bare Ag-605 embedded in PEDOT:PSS layer (**Figure 3**A), which possess

Table 1. Performance of the studied devices under AM 1.5G illumination (100 mW cm^{-2}). The concentration of embedded Ag nanoprisms was the optimized condition. All devices are fabricated in top-illuminated microcavity structures except the normal ITO configurations.

Configuration	J_{sc} (mA cm^{-2})	V_{oc} (V)	FF	PCE (%)[a)]	+[b)]	σ_{mean}[c)]
			On Glass Substrate			
Normal ITO	12.82 ± 0.24	0.96 ± 0.01	0.61 ± 0.01	7.58 ± 0.12 (7.66)	–	1.0%
Reference	14.47 ± 0.24	0.96 ± 0.01	0.60 ± 0.01	8.36 ± 0.16 (8.56)	–	1.7%
Ag-605@SiO_2 (Rear)	15.31 ± 0.30	0.96 ± 0.01	0.60 ± 0.01	8.86 ± 0.20 (9.10)	6.3%	2.1%
Ag-450 (Front)	14.98 ± 0.29	0.96 ± 0.01	0.60 ± 0.01	8.69 ± 0.18 (8.94)	4.4%	1.9%
Dual (Front + Rear)	15.75 ± 0.36	0.96 ± 0.01	0.60 ± 0.01	9.16 ± 0.28 (9.47)	10.6%	2.8%
			On PET Flexible Substrate			
Normal ITO	12.72 ± 0.16	0.96 ± 0.01	0.58 ± 0.01	7.08 ± 0.10 (7.20)	–	1.0%
Reference	14.49 ± 0.25	0.96 ± 0.01	0.59 ± 0.01	8.25 ± 0.17 (8.49)	–	1.1%
Dual	15.79 ± 0.38	0.96 ± 0.01	0.59 ± 0.01	9.05 ± 0.29 (9.36)	10.2%	2.9%

[a)]PCE_{MAX} in the brackets; [b)]The enhancement factors ($\Delta PCE/PCE_{ref}$) of best OPV plasmonic devices compared to that of reference device; [c)]Error values represent the standard deviation of the mean of 25 devices.

severe leaking current in dark *J–V* curves (Figure S6, Supporting Information).[29]

After adapting nanoprisms with a protective silica layer (3 nm), the rear-side Ag-605@SiO_2 device showed an improved PCE of 8.86%, mainly attributed to an enhanced J_{SC} (15.31 mA cm^{-2}). The unchanged V_{oc} and FF compared to the reference device suggested that the doping of Ag nanoprisms into charge transport interlayers poses negligible influence on electrical properties and charge transport, indicating that the enhanced J_{SC} was purely from optical effects. Besides, it is

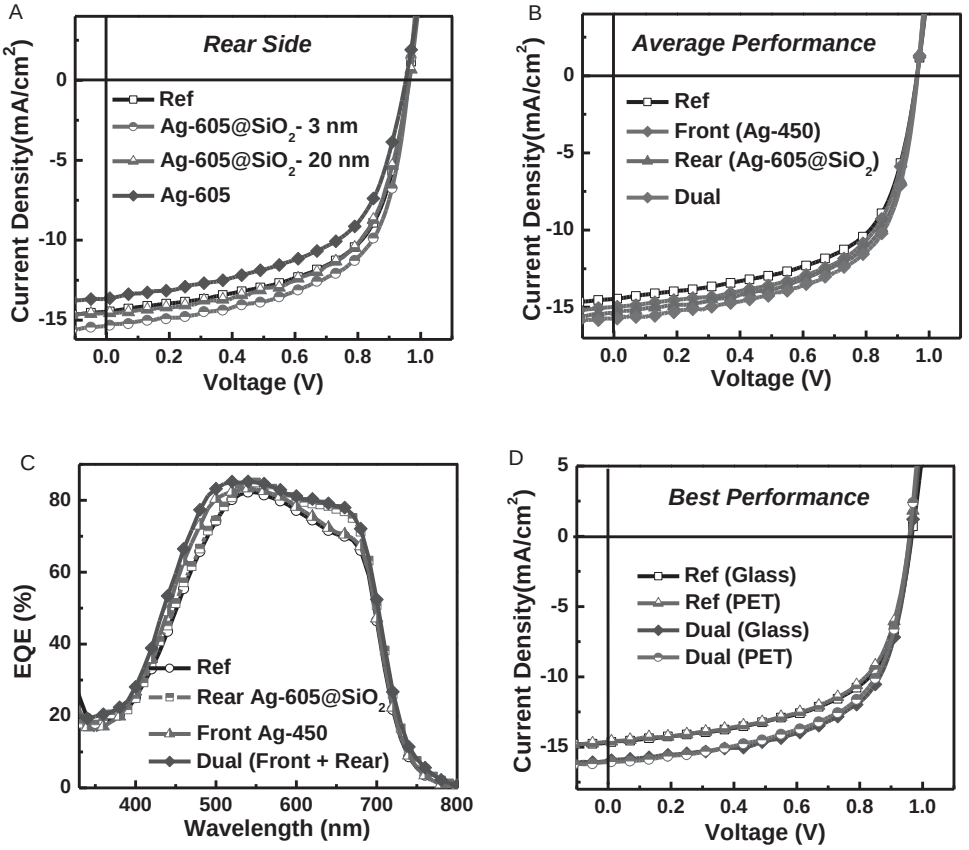

Figure 3. A) *J–V* curves of devices incorporating Ag-605 nanoprisms with various silica-coating thicknesses in PEDOT:PSS layer. B) Average performance and C) external quantum efficiency (EQE) spectra of the studied plasmonic devices with Ag nanoprisms doped in front, rear, and dual charge transport interlayers. D) Best performance of dual plasmonic device on glass and flexible (PET) substrates.

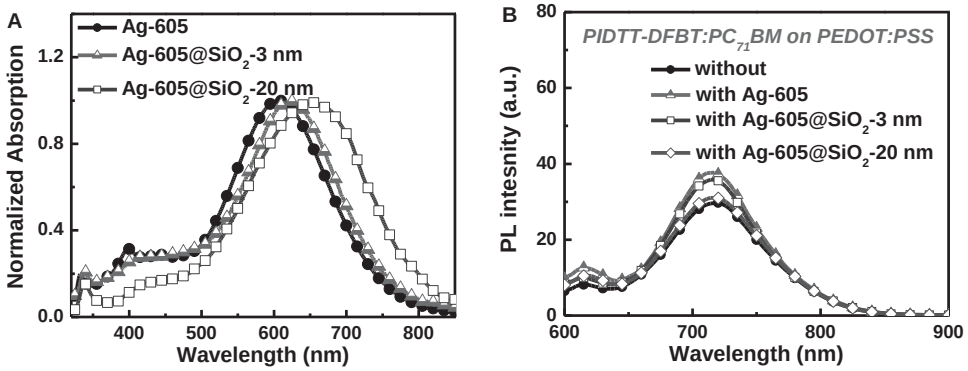

Figure 4. A) UV–Vis spectra of nanoprisms Ag-605 with various silica-coating thicknesses. B) PL spectra of studied BHJ layer spin-coated on PEDOT:PSS that containing different Ag nanoprisms under excited wavelengths at λ_{exc} = 580 nm.

worthwhile to note that the embedded Ag@SiO_2 nanoprisms introduce subtle change on the sheet resistance of interlayer as a result of their low blending concentration. The detailed optimization on blending concentration of studied Ag nanoprisms is summarized in Table S2, Supporting Information, and it revealed that the device performance is dependent on the amount of nanoprisms incorporated in PEDOT:PSS layer.

It is known that the absorption of Ag nanoprisms will further shift to longer wavelength as the thickness of insulating shell increases.[25] As depicted in **Figure 4**A, the Ag-605@SiO_2 (20 nm) showed a red-shifted peak extinction around 650 nm relative to Ag-605@SiO_2 (3 nm). This LSPR region is even more suitable for enhancing light-harvesting of the reference microcavity devices as indicated in the EQE shown in Figure 1. Nevertheless, the plasmonic enhanced in J_{SC} was significantly deteriorated when the thickness of silica shell was increased from 3 nm to 20 nm. Hardly any performance enhancement can be observed in the rear-side Ag-605@SiO_2 (20 nm) device (Figure 3A). These results are inconsistent with the recent finding that P3HT:PCBM films on top of thick silica-protected nanoprisms still showed modestly enhanced polaron yield.[30] We postulated that strong interactions between plasmonic field and excitons instead of far-field scattering effect may dominate the optical enhancement in our microcavity structure device.[17]

It is well documented that LSPR effects can promote the photoexciton formation of the nearby absorbers through the plasmonic near-field effects. The intensity of this local field strongly correlates with the distance between the plasmonic nanostructures and absorbers.[31] To confirm the LSPR effects on optical enhancement, steady state PL measurements were conducted. Figure 4B exhibited the PL spectra of PIDTT-DFBT:PC_{71}BM BHJ on PEDOT:PSS that contains the studied Ag nanoprisms with different thickness of silica shells. In the presence of Ag-605 and Ag-605@SiO_2 (3 nm), the BHJ layer possessed more intense PL intensity relative to the pristine condition. On the contrary, the Ag-605@SiO_2 (20 nm) brought almost no difference on PL intensity since the plasmonic field decayed exponentially with respect to the distance from the surface of Ag nanoprisms.[31] This therefore accounted for the poorer J_{sc} of rear-side Ag-605@SiO_2 (20 nm) devices than the Ag-605@SiO_2 (3 nm) one.

To elucidate the synergistic effects can derive from two (plasmonic and microcavity) optical resonances, control experiments are conducted by changing the extinction peaks of Ag nanoprisms for rear-side doping. The rear-side Ag-530@SiO_2 (3 nm) device only showed a slightly improved PCE of 8.47%, with a J_{sc} of 14.68 mA cm^{-2} (Figure S7, Supporting Information) relative to the reference device (8.36%) while the rear-side Ag-605@SiO_2 (3 nm) device show a significantly enhanced PCE of 8.86% (Table 1). This result indicated that it is difficult to further enhance light absorption if the plasmonic resonance substantially overlaps with the microcavity resonance regions in the combined devices. It can also be realized from the inserted EQE in Figure 1,[13b,21b] where the reference device already possesses high EQE of over 80% in the region around 500–600 nm due to the microcavity resonance effect, suggesting the almost saturated light-harvesting of photoactive layer in this region.

For the front-side plasmonic enhancement, it would be ideal if the light absorption region around 350–500 nm can be increased because of the significant out-of-phase optical loss of the reference device in this region. Thus, Ag-450 nanoprisms with LSPR extinction peak at 450 nm are suitable to be blended into the C_{60}-bis electron-transporting layer to create proper plasmonic resonance. Meanwhile, as previously mentioned, its small edge size (20 nm) is compatible with thin C_{60}-bis layer (15 nm), which can avoid direct contact with Ag electrode. The detailed optimization of blending concentrations on device performance is summarized in Table S3, Supporting Information. At the optimized condition (blending concentration is 1.0 wt%), an improved PCE of 8.69 ± 0.20% can be achieved as compared to the reference device (8.36%) (Figure 3B). Similar to the rear-side plasmonic devices, an increase in J_{sc} (14.47 mA cm^{-2} to 14.98 mA cm^{-2}) contributes to the enhanced PCE.

Given these plasmonic enhancement from both rear and front sides, we next fabricated the dual plasmonic devices by incorporating Ag-450 at front side and Ag-605@SiO_2 at rear side simultaneously in the microcavity configuration.[13b,21b] Very encouragingly, the J_{sc} of such dual device is greatly improved to 15.97 mA cm^{-2}, resulting a PCE_{MAX} of 9.47% (Figure 3B and Table 1). The device performance and enhancement ratios were summarized in Table 1. To understand the contribution of these optical resonance effects in enhanced light-harvesting, the EQE of reference, rear/front-side plasmonic, and dual devices were compared together in Figure 3C. As can be seen, the EQE spectra mainly increased in the region of 400–500 nm and 600–700 nm, corresponding to the front/

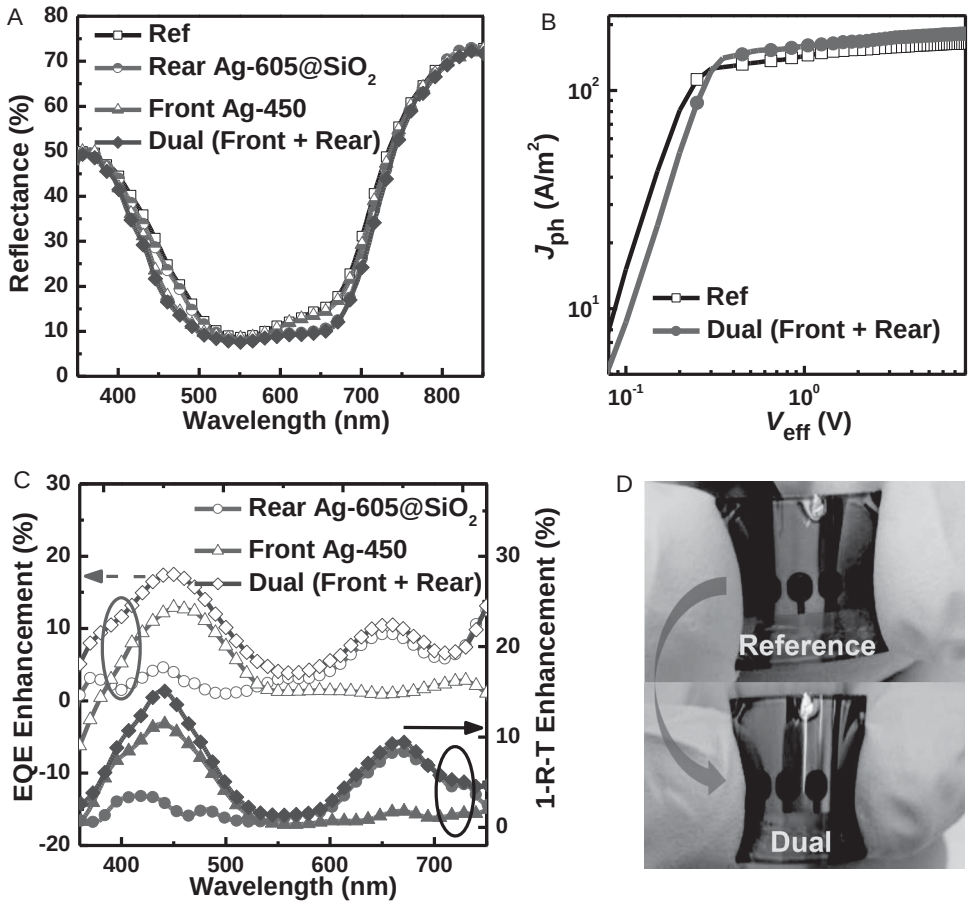

Figure 5. A) Diffuse reflectance spectra of the studied plasmonic devices. B) Photocurrent density (J_{ph}) plotted with respect to the effective voltage (V_{eff}) for the reference and dual plasmonic devices. C) Comparison of enhanced EQE with absorption changes; Left: EQE enhancement factors, $\Delta EQE/EQE_{ref}$ ($\Delta EQE = EQE_{plasmonic} - EQE_{ref}$), Right: the extracted absorption enhancement factors, $\Delta A/A_{ref}$ ($\Delta A = A_{plasmonic} - A_{ref}$). D) Photographs view of color change in authentic ITO-free flexible (PET) devices after embedding Ag nanoprisms into charge transport interlayers.

rear-side plasmonic enhancement, respectively. It suggests the dual plasmonic device showed a combined enhancement in these regions due to the cooperative contributions from embedded nanoprisms with different LSPRs at both sides. It is worth to note that there was only subtle enhancement for all the studied devices at the spectral region between 500 and 600 nm, which affirms that light-harvesting of photoactive layer is almost saturated in this region as discussed.

To further clarify the light-trapping in the dual plasmonic devices, reflectance measurement (R) was conducted to evaluate the absorption (A) within the device, based on equation ($A = 1 - R - T$).[32] As depicted in **Figure 5**A, all plasmonic devices showed lower reflectivity than the reference microcavity device. The extracted absorption of the plasmonic devices in Figure S8, Supporting Information, was clearly increased compared to the reference one. Moreover, the enhancement factor obtained from the extracted absorption is consistent with the EQE enhancement factor (divided by the value of reference device), as presented in Figure 5C. Not only that the spectra of EQE enhancement factor showed similar features (region and intensity) as those of the absorption enhancement factor, but also both of them matched well with the extinction spectra of corresponding embedded nanoprisms. This result demonstrates that we can independently manipulate the plasmon resonances of metal nanoprisms to further enhance the optical properties in various device configurations such as microcavity configuration. By combining these optical resonances (plasmonic and microcavity), an optimal light-harvesting in photoactive layer can be accomplished.

To verify that the increased photocurrent (carrier generation) is derived from enhanced light absorption in our combined system, maximum exciton generation rate (G_{max}) of the devices is calculated and the resulting dependence of photocurrent density (J_{ph}) on the effective voltage (V_{eff}) under illumination at 100 mW cm^{-2} is illustrated in Figure 5B.[33] The log of J_{ph} initially showed a linear relationship to the voltage at low V_{eff} before it levels off and saturates at high V_{eff}. Therefore, we can calculate G_{max} according to the equation $J_{sat} = qG_{max}L$, where q is the electronic charge and L is the thickness of the active layer (≈90 nm). The estimated G_{max} of reference device and dual type device were 1.13×10^{28} m^{-3} s^{-1} (J_{sat} = 163 A m^{-2}) and 1.25×10^{28} m^{-3} s^{-1} (J_{sat} = 180 A m^{-2}), respectively. The enhanced G_{max} (10.6%) is consistent with the enhanced values of PCE and J_{sc} (10.9%). The experiments of light intensity dependent photocurrents were also carried out to gain more insight for the influence of nanoprisms on charge recombination (Figure S9A,

Supporting Information).[34] Both devices yielded the same power law of J_{sc} on the light intensity with factors (*s*) of 0.96. Moreover, the charge transport of both devices remained constant with similar charge mobility, as measured by the space charge-limited current (SCLC) model (Figure S9B, Supporting Information).[35] All these results affirm that the doping of metal nanoprisms into charge transport interlayers has minimal influence on the electrical properties of device, except optical enhancement.

As mentioned earlier, one of the most appealing features of such top-illuminated microcavity ITO-free device is its great potential for making high-efficiency flexible solar cells. Therefore, we have applied this optimized configuration with synergetic optical resonances onto a flexible plastic substrate, poly(ethylene terephthalate) (PET) film. Very impressively, both the reference and combined devices showed higher PCEs than the ITO-based devices, as shown in Figure 3D and Table 1. Similar to the case using rigid glass substrates, the PCE_{MAX} of flexible dual plasmonic device could be increased to 9.36% which is much higher than the reference flexible device (8.49%) due to the significantly improved J_{sc}. The pictures presented in Figure 5D revealed the color change of the authentic devices, indicating the varied light absorption after embedding Ag nanoprisms into the charge-transporting interlayers.

The mechanical properties of these studied flexible ITO-free devices were also examined by testing their bending durability, in which the bending tests were performed by using a cylinder with a bending radius of 0.55 cm. As demonstrated in Figure S10, Supporting Information, both reference and dual devices exhibited decent stability after hundreds of bending cycles while, in stark contrast, the ITO-based devices showed dramatically decreased performance from the first bending cycle and continuous to decrease during the testing.[13a]

3. Conclusions

In summary, we have achieved a highly efficient ITO-free flexible OPV by integrating the plasmonic effects into microcavity configurations. The optimized plasmonic devices incorporating size-dependent Ag nanoprisms blended into both charge-transporting interlayers show a significantly enhanced PCE_{MAX} of 9.4% on flexible substrate. The well-manipulated plasmonic resonances induced by Ag nanoprisms with different LSPR peaks enable the complementary light-harvesting with microcavity resonance in the regions of 400–500 nm and 600–700 nm, resulting in the substantially increased J_{sc}. This result signifies that the spectral matching between the LSPR peaks of Ag nanoprisms and the relatively low absorption response of photoactive layer in the microcavity device is an effective strategy to enhance light-harvesting across its absorption region. In addition, we have also verified that the origin of enhanced PCE is consistent with the enhanced optical absorption by optical measurements. The integration of plasmonic resonances into microcavity configuration revealed in this study not only demonstrates a novel concept to enhance the light-harvesting of OPVs but also pave the way for the practical development of high performance flexible OPVs.

4. Experimental Section

Preparation of Ag Nanoprisms and the Solution: The detailed synthesis of various Ag nanoprisms is presented in the Supporting Information. The Ag nanoprism doped PEDOT:PSS solution was prepared by adding different amounts of a high concentration Ag nanoprism colloid to the PEDOT:PSS aqueous solution. While for the C_{60}-bis doping, various amounts of Ag nanoprisms were blended into the fullerene surfactant in a methanol-based solution.

Device Fabrication and Characterization: For normal ITO-based control devices: ITO-coated substrates (glass or PET (Sigma-Aldrich)) were cleaned sequentially with a detergent, DI-water, acetone, and isopropanol. Prior to the fabrication of the organic layers, the ITO surface was treated with plasma for 20 s. The PEDOT:PSS was spin-coated at 4000 rpm for 30 s, delivering a film thickness of 40–50 nm. Afterwards, PIDTT-DFBT:PC71BM (20 mg mL^{-1}, 1:3, w/w) in a mixture of 1,2-dicholobenzene (o-DCB) and 1-chloronaphthalene (v/v, 97:3) solution was spin-coated on PEDOT:PSS layer at 1000 rpm inside a nitrogen glove box (O_2 and H_2O concentration < 1 ppm), and subsequently dried in a vacuum chamber under nitrogen atmosphere to obtain a film thickness of approximately 90 nm. Then the fullerene surfactant solution was spin-cast under nitrogen atmosphere at 4000 rpm. Finally, silver (100 nm) was thermally evaporated through shadow masks to define a device area of 4.5 mm^2. For the microcavity configuration devices: Plain glass and PET were cleaned via identical cleaning steps and plasma treatment as the ITO-coated substrates and sequentially deposited with 120 nm Ag bottom electrodes. To introduce the plasmonic effects into microcavity device, the Ag nanoprisms were mixed into PEDOT:PSS solution by adding various amounts of concentrated Ag nanoprism colloid solution while different amounts of Ag nanoprisms were blended into the fullerene surfactant in methanol solution before the deposition of each interfacial layers. The aqueous PEDOT:PSS solution with or without nanoprisms was diluted into half concentration by DI-water to deposit a thickness of 25 nm on the Ag substrate. The active layer as well as the C_{60}-bis layer with or without Ag-450 were spin-coated on the PEDOT:PSS using the same conditions as previously mentioned. Top thin Ag electrodes were sequentially evaporated to obtain a thickness of 15 nm. Finally, a TeO_2 capping layer with thickness around 50 nm was deposited on top of thin Ag electrode via thermal evaporation using the same mask. A Keithley 2400 source meter unit was used to record *J-V* characteristics in this study. A 300 W xenon arc solar simulator equipped with an AM 1.5G filter was used to simulate a light intensity of 100 mW cm^{-2}. The illumination intensity of the light source was accurately calibrated employing a standard Si photodiode detector equipped with a KG-5 filter, which can be traced back to the standard cell of the National Renewable Energy Laboratory (NREL). The EQE spectra performed here were obtained from an IPCE setup consisting of a Xenon lamp (Oriel, 450 W) as the light source, a monochromator, a chopper with a frequency of 100 Hz, a lock-in amplifier (SR830, Stanford Research Corp), and a Si-based diode (J115711–1-Si detector) for calibration. The calculated J_{sc} values obtained by integrating the EQE spectrum under the AM 1.5G illumination condition agreed well with the measured J_{sc} value from *J-V* characteristics and the differences were within 4%.

Supporting Information

Supporting Information is available from the Wiley Online Library or from the author.

Acknowledgements

The authors thank the financial support from the Air Force Office of Scientific Research (FA9550–09–1–0426), the Asian Office of Aerospace R&D (FA2386–11–1–4072), and the Office of Naval Research (N00014–

14–1–0170). A. K.-Y. Jen thanks the Boeing Foundation for financial support. K. Yao thanks the State-Sponsored Scholarship for Graduate Students from China Scholarship Council.

Received: September 22, 2014
Revised: October 31, 2014
Published online: December 6, 2014

[1] N. Camaioni, R. Po, *J. Phys. Chem. Lett.* **2013**, *4*, 1821.
[2] a) D.-H. Ko, J. R. Tumbleston, A. Gadisa, M. Aryal, Y. Liu, R. Lopez, E. T. Samulski, *J. Mater. Chem.* **2011**, *21*, 16293; b) W. Yuan, H. Zhao, H. Hu, S. Wang, G. L. Baker, *ACS Appl. Mater. Interfaces* **2013**, *5*, 4155.
[3] a) J. Y. Kim, K. Lee, N. E. Coates, D. Moses, T. Q. Nguyen, M. Dante, A. J. Heeger, *Science* **2007**, *317*, 222; b) J. You, L. Dou, K. Yoshimura, T. Kato, K. Ohya, T. Moriarty, K. Emery, C. C. Chen, J. Gao, G. Li, Y. Yang, *Nat. Commun.* **2013**, *4*, 1446.
[4] R. Betancur, P. Romero-Gomez, A. Martinez-Otero, X. Elias, M. Maymó, J. Martorell, *Nat. Photonics* **2013**, *7*, 995.
[5] H. Wu, D. Kong, Z. Ruan, P. C. Hsu, S. Wang, Z. Yu, T. J. Carney, L. Hu, S. Fan, Y. Cui, *Nat. Nanotechnol.* **2013**, *8*, 421.
[6] J. Lee, S.-Y. Kim, C. Kim, J.-J. Kim, *Appl. Phys. Lett.* **2010**, *97*, 083306.
[7] a) H. W. Lin, S. W. Chiu, L. Y. Lin, Z. Y. Hung, Y. H. Chen, F. Lin, K. T. Wong, *Adv. Mater.* **2012**, *24*, 2269; b) Y. H. Chen, C. W. Chen, Z. Y. Huang, W. C. Lin, F. Lin, K. T. Wong, H. W. Lin, *Adv. Mater.* **2014**, *26*, 1129.
[8] a) H. A. Atwater, A. Polman, *Nat. Mater.* **2010**, *9*, 205; b) S. S. Kim, S. I. Na, J. Jo, D. Y. Kim, Y. C. Nah, *Appl. Phys. Lett.* **2008**, *93*, 073307.
[9] V. Mihailetchi, L. Koster, J. Hummelen, P. Blom, *Phys. Rev. Lett.* **2004**, *93*, 216601.
[10] a) X. Guo, N. Zhou, S. J. Lou, J. Smith, D. B. Tice, J. W. Hennek, R. P. Ortiz, J. T. L. Navarrete, S. Li, J. Strzalka, L. X. Chen, R. P. H. Chang, A. Facchetti, T. J. Marks, *Nat. Photonics* **2013**, *7*, 825; b) C. Cabanetos, A. El Labban, J. A. Bartelt, J. D. Douglas, W. R. Mateker, J. M. Frechet, M. D. McGehee, P. M. Beaujuge, *J. Am. Chem. Soc.* **2013**, *135*, 4656; c) L. Dou, J. You, Z. Hong, Z. Xu, G. Li, R. A. Street, Y. Yang, *Adv. Mater.* **2013**, *25*, 6642.
[11] Y. Long, *Appl. Phys. Lett.* **2009**, *95*, 193301.
[12] M. Agrawal, P. Peumans, *Opt. Express* **2008**, *16*, 5385.
[13] a) J. F. Salinas, H. L. Yip, C. C. Chueh, C. Z. Li, J. L. Maldonado, A. K. Jen, *Adv. Mater.* **2012**, *24*, 6362; b) K. S. Chen, H. L. Yip, J. F. Salinas, Y. X. Xu, C. C. Chueh, A. K. Jen, *Adv. Mater.* **2014**, *26*, 3349.
[14] K. Ellmer, *Nat. Photonics* **2012**, *6*, 809.
[15] a) K. S. Chen, J. F. Salinas, H. L. Yip, L. J. Huo, J. H. Hou, A. K. Jen, *Energy Environ. Sci.* **2012**, *5*, 9551; b) C. C. Chueh, S. C. Chien, H. L. Yip, J. F. Salinas, C. Z. Li, K. S. Chen, F. C. Chen, W. C. Chen, A. K. Jen, *Adv. Energy Mater.* **2013**, *3*, 417.
[16] Y. H. Chen, C. W. Chen, Z. Y. Huang, W. C. Lin, L. Y. Lin, F. Lin, K. T. Wong, H. W. Lin, *Adv. Mater.* **2014**, *26*, 1129.
[17] J. L. Wu, F. C. Chen, Y. S. Hsiao, F. C. Chien, P. Chen, C. H. Kuo, M. H. Huang, C. S. Hsu, *ACS Nano* **2011**, *5*, 959.
[18] L. J. Sherry, R. Jin, C. A. Mirkin, G. C. Schatz, R. P. Van Duyne, *Nano Lett.* **2006**, *6*, 2060.
[19] K. R. Catchpole, A. Polman, *Appl. Phys. Lett.* **2008**, *93*, 191113.
[20] a) V. Jankovic, Y. M. Yang, J. You, L. Dou, Y. Liu, P. Cheung, J. P. Chang, Y. Yang, *ACS Nano* **2013**, *7*, 3815; b) L. Lu, Z. Luo, T. Xu, L. Yu, *Nano Lett.* **2013**, *13*, 59.
[21] a) X. Yang, C. C. Chueh, C. Z. Li, H. L. Yip, P. P. Yin, H. Z. Chen, W. C. Chen, A. K. Y. Jen, *Adv. Energy Mater.* **2013**, *3*, 666; b) K. Yao, M. Salvador, C. C. Chueh, X. K. Xin, Y. X. Xu, D. W. deQuilettes, T. Hu, Y. Chen, D. S. Ginger, A. K. Y. Jen, *Adv. Energy Mater.* **2014**, *4*, 1400206.
[22] a) C. Z. Li, C. C. Chueh, H. L. Yip, K. M. O'Malley, W. C. Chen, A. K. Y. Jen, *J. Mater. Chem.* **2012**, *22*, 8574; b) Y. X. Xu, C. C. Chueh, H. L. Yip, F. Z. Ding, Y. X. Li, C. Z. Li, X. Li, W. C. Chen, A. K. Y. Jen, *Adv. Mater.* **2012**, *24*, 6356.
[23] D. Aherne, D. M. Ledwith, M. Gara, J. M. Kelly, *Adv. Funct. Mater.* **2008**, *18*, 2005.
[24] A. P. Kulkarni, K. M. Noone, K. Munechika, S. R. Guyer, D. S. Ginger, *Nano Lett.* **2010**, *10*, 1501.
[25] J. Rodríguez-Fernández, I. Pastoriza-Santos, J. Pérez-Juste, F. J. García de Abajo, L. M. Liz-Marzán, *J. Phys. Chem. C* **2007**, *111*, 13361.
[26] H. Choi, S. J. Ko, Y. Choi, P. Joo, T. Kim, B. R. Lee, J. W. Jung, H. J. Choi, M. Cha, J. R. Jeong, I. W. Hwang, M. H. Song, B. S. Kim, J. Y. Kim, *Nat. Photonics* **2013**, *7*, 732.
[27] H. Jin, C. Tao, M. Velusamy, M. Aljada, Y. Zhang, M. Hambsch, P. L. Burn, P. Meredith, *Adv. Mater.* **2012**, *24*, 2572.
[28] S. W. Baek, J. Noh, C. H. Lee, B. Kim, M. K. Seo, J. Y. Lee, *Sci. Rep.* **2013**, *3*, 1726.
[29] a) H. Choi, J. P. Lee, S. J. Ko, J. W. Jung, H. Park, S. Yoo, O. Park, J. R. Jeong, S. Park, J. Y. Kim, *Nano Lett.* **2013**, *13*, 2204; b) B. Wu, X. Wu, C. Guan, K. Fai Tai, E. K. L. Yeow, H. Jin Fan, N. Mathews, T. C. Sum, *Nat. Commun.* **2013**, *4*, 2004.
[30] M. Salvador, B. A. MacLeod, A. Hess, A. P. Kulkarni, K. Munechika, J. I. Chen, D. S. Ginger, *ACS Nano* **2012**, *6*, 10024.
[31] a) P. Anger, P. Bharadwaj, L. Novotny, *Phys. Rev. Lett.* **2006**, *96*, 113002; b) S. D. Standridge, G. C. Schatz, J. T. Hupp, *J. Am. Chem. Soc.* **2009**, *131*, 8407.
[32] X. Li, W. C. Choy, L. Huo, F. Xie, W. E. Sha, B. Ding, X. Guo, Y. Li, J. Hou, J. You, Y. Yang, *Adv. Mater.* **2012**, *24*, 3046.
[33] V. D. Mihailetchi, H. X. Xie, B. de Boer, L. J. A. Koster, P. W. M. Blom, *Adv. Funct. Mater.* **2006**, *16*, 699.
[34] S. R. Cowan, A. Roy, A. J. Heeger, *Phys. Rev. B* **2010**, *82*, 245207.
[35] V. Mihailetchi, J. Wildeman, P. Blom, *Phys. Rev. Lett.* **2005**, *94*, 126602.